The Astrophysical Journal Letters, 769:L11 (5pp), 2013 May 20 doi:10.1088/2041-8205/769/1/L11

CORONAL THICK TARGET HARD X-RAY EMISSIONS AND RADIO EMISSIONS

Jeongwoo Lee[1,2], Daye Lim[2], G. S. Choe[2], Kap-Sung Kim[2], and Minhwan Jang[3]
[1] Physics Department, New Jersey Institute of Technology, Newark, NJ 07102, USA
[2] School of Space Research, Kyung Hee University, Yongin 446-701, Korea
[3] Department of Astronomy and Space Science, Kyung Hee University, Yongin 446-701, Korea
Received 2013 March 17; accepted 2013 April 15; published 2013 May 7

ABSTRACT

A distinctive class of hard X-ray (HXR) sources located in the corona was recently found, which implies that the collisionally thick target model (CTTM) applies even to the corona. We investigated whether this idea can be independently verified by microwave radiations which have been known as the best companion to HXRs. This study is conducted on the *GOES* M2.3 class flare which occurred on 2002 September 9 and was observed by the *Reuven Ramaty High-Energy Solar Spectroscopic Imager* and the Owens Valley Solar Array. Interpreting the observed energy-dependent variation of HXR source size under the CTTM, the coronal density should be as high as 5×10^{11} cm^{-3} over a distance of up to 12″. To explain the cutoff feature of the microwave spectrum at 3 GHz, however, we require a density no higher than 1×10^{11} cm^{-3}. Additional constraints must be placed on the temperature and magnetic field of the coronal source in order to reproduce the microwave spectrum as a whole. First, a spectral feature called the Razin suppression requires a magnetic field in a range of 250–350 G along with high viewing angles around 75°. Second, to avoid excess fluxes at high frequencies due to the free–free emission that was not observed, we need a high temperature $\geqslant 2 \times 10^7$ K. These two microwave spectral features, Razin suppression and free–free emissions, become more significant at regions of high thermal plasma density and are essential for validating and determining additional parameters of the coronal HXR sources.

Key words: Sun: flares – Sun: particle emission – Sun: radio radiation – Sun: X-rays, gamma rays

1. INTRODUCTION

Observations of hard X-ray (HXR) bursts with the *Reuven Ramaty High-Energy Solar Spectroscopic Imager* (*RHESSI*) have produced a number of new properties of high-energy electrons accelerated during solar flares. One of its recent discoveries is a distinctive type of flare in which the bulk of the HXR emission is from the coronal part of the loop (Veronig & Brown 2004; Sui et al. 2004; Krucker et al. 2008). For such sources, the corona can be considered not only as the site of particle acceleration, but as a thick target stopping the accelerated electrons before they can penetrate the chromosphere. This is in contrast with the traditional idea of the collisional thick target model (CTTM) which was believed to apply only to the dense chromosphere. Veronig & Brown (2004) studied two events for which the coronal densities of the flaring loops were found sufficiently high to justify the CTTM. Xu et al. (2008) showed that for a certain group of events the observed coronal HXR source extent varies with photon energy, as expected from a CTTM with an extended acceleration region in the coronal loop. The result not only serves as evidence for the coronal CTTM, but also allows estimates of the plasma density and longitudinal extent of the acceleration region. Guo et al. (2012a) carried out similar work but used the electron flux images instead of photon maps, as constructed by regularized spectral inversion of the visibility data in the count domain (Piana et al. 2007). Guo et al. (2012b) further related those interpretations to the number of particles within the acceleration region, the filling factor, and the specific acceleration rate in units of electrons per second and per ambient electron. According to these studies, those events with coronal thick target HXR sources form an important (though small) class of solar flares for which acceleration parameters can directly be inferred.

If we plan to test the CTTM for coronal HXR sources using other forms of radiation, microwave radiation should be the first choice for its close relationship to HXRs. Time profiles of microwave emissions tend to show a peak-to-peak correlation with HXR light curves, which led to the idea that the same population of electrons is responsible for both types of radiation (e.g., Dulk 1985). Spatially, both emissions should arise, at least, from the same magnetic loop or loop systems, but the location of each radiation maximum may differ along the loop as their radiation efficiencies respond differently to plasma parameters and magnetic fields (e.g., Sakao et al. 1996). We expect that the microwave spectrum will be particularly important in relation to the studies of the coronal CTTM. The main microwave radiation mechanism, gyrosynchrotron radiation, has primarily served as a diagnostic for magnetic field and electron distribution. However, when thermal density is very high, two spectral features sensitive to density, the Razin suppression (Razin 1960) and free–free emission, become prominent. The Razin suppression refers to less efficient radiation in the presence of ambient medium compared with the radiation in vacuum, and the Razin frequency below which the effect is significant is given by $\nu_R \approx 20n/B_\perp$ Hz, where n is the electron density in units of cm^{-3} and $B_\perp$ is the transverse magnetic field component in gauss (Dulk 1985). The Razin suppression will thus be effective for the condition of thick target loop-top HXR sources. The well-known free–free opacity is proportional to $n^2 T^{-1/2}$, with T being the plasma temperature. In addition, there is an *absolute* cutoff of microwave radiation at the plasma frequency which is a sole function of plasma density (see, e.g., Ramaty 1969; Melrose 1980). With these features that become prominent at high density, a microwave spectrum should play a critical role in validating the CTTM applied to coronal sources.

In this Letter, we compare the properties of a coronal HXR source with those of a microwave source detected in an event that we consider to be a candidate for the coronal thick target source. The event is the 2002 September 9 flare that occurred in NOAA AR 0105 and acquired a *GOES* soft X-ray class of M2.3.

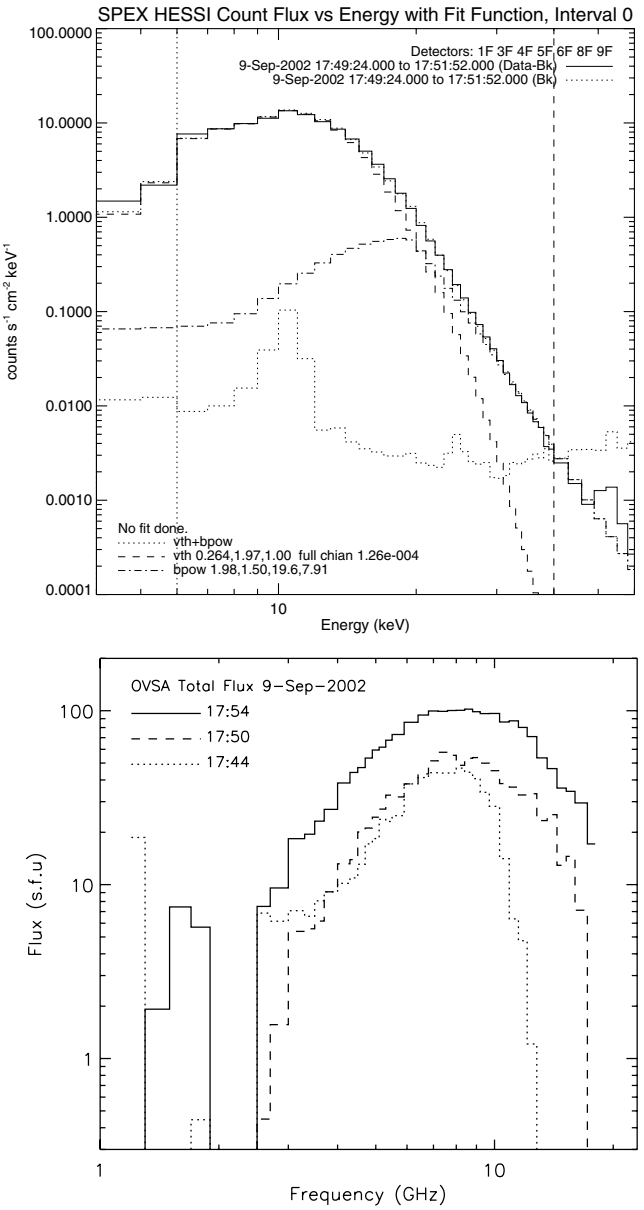

Figure 1. Top panel: a *RHESSI* spectrum for the flare on 2002 September 9. A spectral fit is made for the interval 17:49:23–17:51:53 UT. The thermal component of the spectrum (dashed histogram) has a temperature of 1.97 keV and the nonthermal component (dot-dashed) has transition energy at 19.6 keV and spectral index $\gamma = 7.91$. The sum of the thermal and nonthermal components (solid histogram) and the background is also shown. Bottom panel: the OVSA microwave spectra at three different time intervals as denoted are shown.

This event was observed by *RHESSI* and the Owens Valley Solar Array (OVSA) and is one of the rare events for which spatial and spectral information at both wavelengths is available for this type of study.

2. SPECTRA OF HXR AND MICROWAVES

In Figure 1, we show the *RHESSI* and OVSA spectra during the 2002 September 9 flare. The top panel shows the spatially integrated *RHESSI* spectrum at a single time corresponding to a maximum emission measure obtained using OSPEX in the SolarSoftWare (SSW). Ji et al. (2004) carried out the imaging spectroscopy for the same event. In their result and also in ours (Figure 2), the *RHESSI* source appears to be a single source and the spectra obtained through OSPEX are indeed

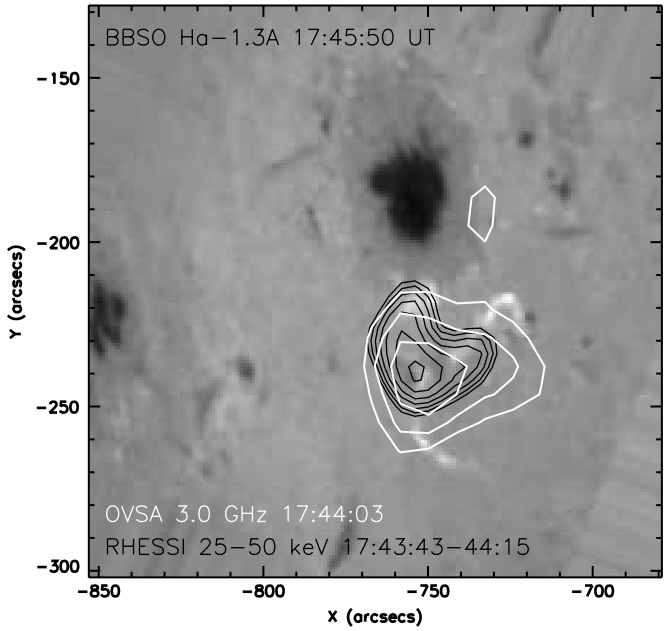

Figure 2. The 25–50 keV *RHESSI* source (black contours) and the OVSA microwave source (white contours) in comparison with the Hα blue wing image (background grayscale image) from the BBSO. These images are chosen to be near one of the flare peak times 17:44 UT.

similar to those obtained from the imaging spectroscopy. As a characteristic feature, the spectrum shows steeply decreasing flux with increasing photon energy with spectral indices as high as $7 \leqslant \gamma \leqslant 8$. Such a high index is typical for the events classified for the coronal thick target HXR sources (Guo et al. 2012a, 2012b; Xu et al. 2008). The spectral index γ will later be used to provide information on electron energy distribution for the modeling of the HXR source loop and that of the microwave spectra. In spite of such a soft nonthermal component, a thermal component could still be identified and the maximum temperature is found to be $T \approx 2 \times 10^7$ K at around 17:50 UT, close to what we infer from the *GOES* soft X-ray data.

The bottom panel shows the total power microwave spectra for the 2002 September 9 flare at three selected times. This is one of the calibrated microwave spectra in the period of 2001–2003 that can be downloaded from the OVSA Web site. Like the HXR spectra, these microwave spectra are also spatially integrated and include both R and L polarizations added together. They appear in a typical shape, but with rapidly falling fluxes toward decreasing frequencies, which can be a sign for the Razin suppression, and is suggestive of a high coronal density. The high-frequency spectrum is steeply decreasing with increasing frequency, which is qualitatively consistent with the high photon spectral index of the *RHESSI* spectrum as found above. We also note that the peak frequency of the microwave spectrum does not change much in the course of the flare. Previously, Belkora (1997) claimed that such a feature may indicate the effect of the Razin suppression. It is thus qualitatively arguable that the spectral morphology of the OVSA spectra is supportive of the high coronal density required for the CTTM of the coronal HXR source.

3. HXR AND MICROWAVE MAPS

The OVSA imaging procedure is less known compared with that of *RHESSI*. Since OVSA uses many frequencies, all-night observations of a quasar point source such as 3C84

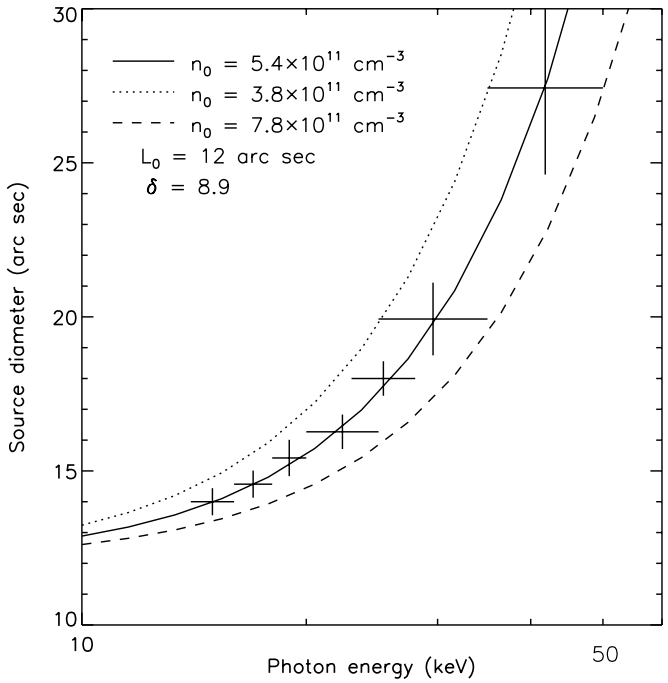

Figure 3. Model fits to the longitudinal dimension of the HXR source. We calculate models (lines) by varying ambient density n_0 and the initial length of the trap L_0 to fit the observed HXR source dimension (crosses) at seven photon energies.

are made several times a year, and are used to calibrate solar data obtained at nearby times. Daily calibration observations at selected frequencies are also made to provide corrections to the above calibration. The calibrated visibilities are fed into the *wimagr* program available in the SSW, after which the imaging can be performed in a procedure very similar to that of the Astronomical Image Processing System.

Figure 2 shows HXR and microwave maps as contours on top of an Hα off-band blue-wing image obtained from the Big Bear Solar Observatory (BBSO). Based on the steep HXR spectrum and the noise level (Figure 1), the HXR imaging was performed below 50 keV. Within the energy range only a single loop-top source was found. Microwave sources generally vary with frequency more significantly, but the centroid of a 3.0 GHz microwave source is cospatial with that of the 25–50 keV HXR source as shown in this figure. Both the HXR and microwave sources appear as a single source lying between the two Hα kernels, and their morphologies change only a little with time (for more details on the morphology of this event, see Ji et al. 2004 and Lee et al. 2006). We thus regard the HXR source as a loop-top coronal thick target source (cf. Veronig & Brown 2004). We followed the technique of Xu et al. (2008) to determine the source sizes using the Vis-Forward fitting and made a model fit to the observed HXR source size as a function of photon energy. As for the model, we actually used Equation (5) of Guo et al. (2012b), which corresponds to Xu et al.'s (2008) model with an extended acceleration region of length, L_0, uniformly filled with dense material of density n_0. This model also includes the electron energy distribution with a power-law index for which we use $\delta = \gamma + 1 = 8.9$ under the thick target bremsstrahlung approximation (Brown 1971). Figure 3 shows our fitting of the model to the observed HXR source size (symbols) at seven photon energies by varying n_0 and L_0. We obtained $n_0 = (5.4 \pm 1.6) \times 10^{11}$ cm^{-3} and $L_0 \approx 12''$ from these data.

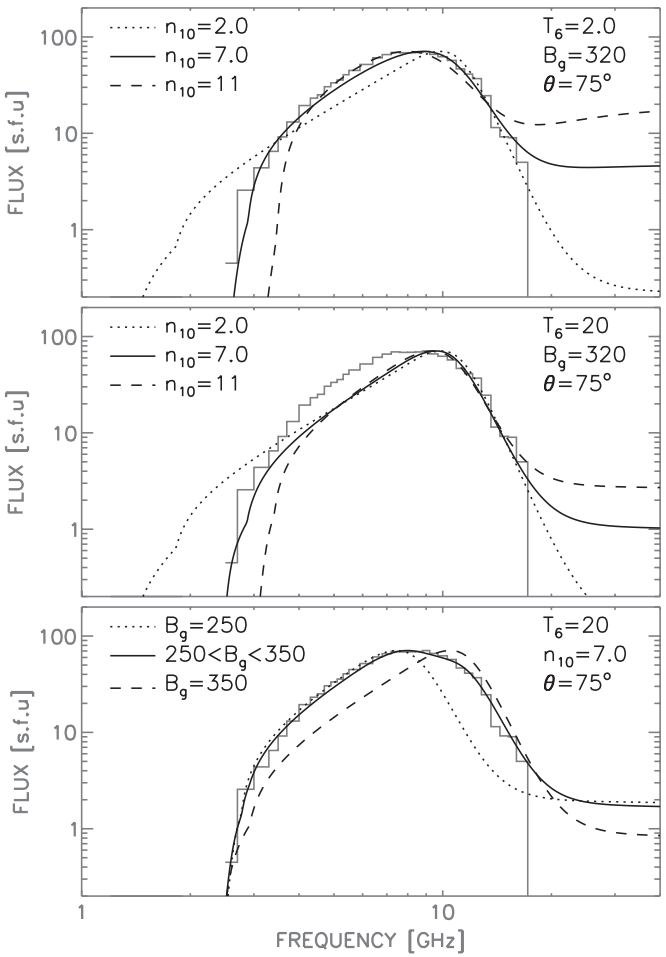

Figure 4. Model fits to an OVSA spectrum observed at 17:50:30 UT. The OVSA spectrum is shown as a histogram. The model parameters denoted are n_{10} (density in units of 10^{10} cm^{-3}), T_6 (temperature in 10^6 K), and B_g (magnetic field in gauss). Top panel: three densities are adopted to show how the spectrum varies with density. Middle panel: the same model parameters as in the top panel are used except that T is raised to 10 times higher. Bottom panel: two models with weaker (stronger) magnetic fields (dotted and dashed lines) are averaged to give an inhomogeneous model (solid line).

4. MODEL FITS TO THE OVSA SPECTRA

We calculated a set of theoretical microwave spectra for comparison with the OVSA spectrum using the numerical code developed by Fleishman & Kuznetsov (2010), which includes full treatment of the Razin effect. In Figure 4, we show our search for the best set of model parameters with which we can reproduce the OVSA spectrum at the time of the maximum density (~17:50 UT) chosen as a representative spectrum. In the top panel we first tried a modest density 2.1×10^{10} cm^{-3} and the same electron energy distribution derived from the *RHESSI* spectrum, i.e., $\delta = 8.9$, except that the electron energy distribution is assumed to extend up to 1 MeV. This model (shown as the dotted line in the top panel) reproduces the high-frequency spectrum to some extent, but fails to match the low-frequency spectrum. If a homogeneous model predicted a more rapidly increasing spectrum at low frequencies than observed, we may suspect that the disagreement is due to source inhomogeneity in reality (e.g., Lee et al. 1994). In this case, however, the model predicts a more extended spectrum toward lower frequencies than observed. We thus adjusted other factors maintaining the homogeneous

source assumption. With a higher density 7×10^{10} cm^{-3}, the model (solid line) reproduces the low-frequency slope under the enhanced Razin suppression. It closely fits to the high-frequency spectrum as well, except somewhat excessive fluxes are predicted at the highest observed frequencies. If we further raise the density as desired for supporting the thick target HXR source, we end up with a disagreement between the model (dashed line) and observation at both low and high frequencies, unfortunately.

At this point we should clarify one basic limitation encountered in the current modeling. Even though we will further adjust other parameters to reproduce the microwave spectrum more closely, the density requirement for this microwave spectrum is rather strict. That is, the minimum cutoff frequency for microwave radiation is the local plasma frequency, a sole function of density. More specifically, the *o*-mode is cut off at local plasma frequency and *x*-mode at a higher frequency that depends on the magnetic field as well (Melrose 1980). Since this spectrum starts above 3 GHz, we derive $n \leqslant 1 \times 10^{11}$ cm^{-3}. Admittedly, this density is a few factors lower than that needed to explain the HXR source dimension varying with energy under the CTTM, and this limit value of density cannot be adjusted by changes of other parameters.

We now proceed with the "lowered" target value of density. Since the excessive fluxes at high frequencies are due to free–free emission, we adopted higher temperatures as a way of suppressing the free–free emission. The three models shown in the middle panel inherit the same parameters from those in the top panel except the temperature increased to 2×10^7 K. At this high temperature, the high-frequency fluxes are significantly *reduced*, and all models agree to the observed spectrum at high frequencies. We may further increase temperature without loosing this success, but too high a temperature is unwanted from a physical point of view because the medium should be a cold target for Coulomb collisions. Emslie (2003) quantified the condition for a cold target as $E > 5kT$, where E is the electron energy and T is the target temperature. Kosugi et al. (1988) have shown that the electrons producing photons at ϵ have energies in the range $1 < E/\epsilon < 3$. Since we concern ourselves with the *RHESSI* spectrum above 6 keV, the temperature 2×10^7 K or 2 keV may qualify as a cold target. However, T cannot be much higher than this, especially considering that this photon spectrum is very soft and E could be close to ϵ. For instance, $E/\epsilon < 2$ gives $T < 2.4 \times 10^7$ K for cold target.

In the above, change of the temperature helped to fit the high-frequency spectrum, but now these models no longer fit the low-frequency spectrum. To solve this problem, we adjust the magnetic field B. In general, increasing (decreasing) B results in a shift of the spectrum to higher (lower) frequencies. Two models calculated with $B = 250$ G and 350 G are respectively shown as the dotted and dashed lines in the bottom panel. Each individual model spectrum appears to be narrower than the observed spectrum. The low (high) field strength model could, however, reproduce the low (high) frequency spectrum. We thus created an average model (solid line) of these two by linearly summing the flux from each model, which well agrees to the observed spectrum overall. We thus conclude that the source must have an inhomogeneous magnetic field distribution in the range of 250 G $\leqslant B \leqslant$ 350 G. The viewing angle of magnetic field, θ, is another variable and this should be high. Otherwise, the free–free emission tends to compete with the gyrosynchrotron radiation, which is unwanted in this case. An extensive exercise shows that a high viewing angle is preferred, and we have fixed θ to 75° throughout this modeling. All these calculations were made with the isotropic pitch angle distribution of electrons. If it were significantly anisotropic, the resulting spectral morphology may differ from the present result even for the same electron energy distribution (Lee & Gary 2000). In that case, a few more assumptions regarding the electron energy distribution will be needed, which we do not regard as essential for the current study.

5. CONCLUDING REMARKS

We have studied the HXR and microwave data of the 2002 September 9 flare with a goal of testing the coronal thick target hypothesis for HXR sources based on the accompanying microwave spectra. Our study found that the microwave spectrum provides strong constraints on the thick target interpretation of HXR sources. First, the lowest frequency of the microwave spectrum is strictly determined by the local plasma density, and the derived density $\leqslant 1 \times 10^{11}$ cm^{-3} is close to, but five times lower than, the density found from the energy-dependent variation of the coronal HXR source. In addition to the density, a temperature $\geqslant$2 keV and a magnetic field strength, 250–350 G, are also required, which will again be constrained by the condition for a cold target for bremsstrahlung and the measurement of the photospheric magnetic field, respectively.

The next question will be whether these constraints could be alleviated by introducing a more realistic, inhomogeneous density structure instead of the simplified assumption for a uniform density source. We commonly consider a source of dense and tenuous regions mixed, i.e., filamentary structure, in which case the tenuous regions filled with nonthermal electrons work as microwave sources and the dense regions as thick target HXR sources. This scenario is not necessarily promising because microwaves should propagate through the dense plasma and cannot avoid the highly enhanced free–free opacity. The next conceivable structure is an inhomogeneous loop along its length such that a section in loop top is tenuous, and the rest is filled with dense materials working as a thick target to Coulomb collisions (Xu et al. 2008). This model is actually favorable for explaining the microwave source, but has to be disputed because it is in apparent conflict with the HXR source lying in the loop top. In our current idea, the only plausible case would be a somewhat arbitrary coaxial loop structure which consists of the inner loop filled with dense colder plasma and the outer one with tenuous and hot plasma, so that the former is ideal for the thick target HXR source and the latter is more favorable for the microwave emission. In this case the small disagreement between the densities derived from microwaves and HXRs, respectively, could be made acceptable. This scenario would, however, need an explanation as to why the inner core has dense and colder materials compared with the outer part of the loop.

In summary, a microwave spectrum provides unique constraints on the coronal HXR sources through the cutoff frequency, the cold target temperature, the free–free opacity, and the Razin effect. These constraints are related to the fundamental physics and are thus robust. Microwave spectral observations should therefore be regarded as a new asset for validating those events of the coronal HXR sources and for determining additional source conditions for them that were not available from HXR observations alone. Future studies may benefit from the use of microwave polarizations and time profiles that will further enhance the diagnostic capabilities.

We thank the *RHESSI* team for an excellent data set. This work was supported by the WCU Program through NRF funded by MEST of Korea (R31-10016). J.L. was supported by the International Scholarship of Kyung Hee University, and also by NASA grants NNX11AB49G and NAS5-01072 (NA03) 937836 to NJIT. G.S.C. was supported by the Korea Research Foundation grant funded by the Korean Government (KRF-2007-313-C00324). M.J. thanks the Kyung Hee University for granting him a sabbatical, during which his part of this research was performed.

REFERENCES

Belkora, L. 1997, ApJ, 481, 532
Brown, J. C. 1971, SoPh, 18, 489
Dulk, G. A. 1985, ARA&A, 23, 169
Emslie, A. G. 2003, ApJL, 595, L119
Fleishman, G. D., & Kuznetsov, A. A. 2010, ApJ, 721, 1127
Guo, J., Emslie, A. G., Kontar, E. P., et al. 2012a, A&A, 543, 53
Guo, J., Emslie, A. G., Massone, A. M., & Piana, M. 2012b, ApJ, 755, 32
Ji, H., Wang, H., Schmahl, E. J., Qiu, J., & Zhang, Y. 2004, ApJ, 605, 938
Kosugi, T., Dennis, B. R., & Kai, K. 1988, ApJ, 324, 1118
Krucker, S., Hurford, G. J., MacKinnon, A. L., Shih, A. Y., & Lin, R. P. 2008, ApJ, 678, 63
Lee, J., & Gary, D. E. 2000, ApJ, 543, 457
Lee, J., Gary, D. E., & Choe, G. S. 2006, ApJ, 647, 638
Lee, J., Gary, D. E., & Zirin, H. 1994, SoPh, 152, 409
Melrose, D. B. 1980, Plasma Astrophysics (New York: Gordon and Breach)
Piana, M., Massone, A. M., Hurford, G. J., et al. 2007, ApJ, 665, 846
Ramaty, R. 1969, ApJ, 158, 753
Razin, V. A. 1960, IzRad, 3, 584
Sakao, T., Kosugi, T., Masuda, S., et al. 1996, AdSpR, 17, 67
Sui, L., Holman, G. D., & Dennis, B. R. 2004, ApJ, 612, 546
Veronig, A., & Brown, J. 2004, ApJL, 603, L117
Xu, Y., Emslie, A. G., & Hurford, G. J. 2008, ApJ, 673, 576